Structural and Phenomenological Characterization of the Thermoreversible Sol−Gel Transition of a Zirconyl Aqueous Precursor Modified by Sulfuric Acid

L. A. Chiavacci, S. H. Pulcinelli,* and C. V. Santilli

Instituto de Química, UNESP, P.O. Box 355, 14801-970 Araraquara SP, Brazil

V. Briois

LURE, UPS, Bât 209D, 91405 Orsay Cedex, France

Received May 28, 1997. Revised Manuscript Received February 10, 1998

The thermoreversible sol−gel transition is well-known in biological and organic polymeric systems but has not been reported for inorganic systems. In this paper we put in evidence a thermoreversible sol−gel transition for zirconyl chloride aqueous solutions modified by sulfuric acid in the ratio 3:1 $Zr:SO_4$. The synthesis conditions are detailed and a variety of experimental techniques (turbidimetry, dynamic rheology, and EXAFS) have been employed for investigating the thermal reversibility and the chemical structure of this new material. Turbidimetric measurements performed for solutions containing different concentrations of precursor have evidenced that the sol−gel transformation temperature increases from 50 to 80 °C as the concentration of zirconyl chloride decreases from 0.22 to 0.018 mol L^{-1}. A more detailed study has been done for the sample with [Zr] = 0.156 mol L^{-1}, in which the sol−gel−sol transformation has been repeated several times by a cyclic variation of the temperature. The mechanical properties of this sample, evaluated by measuring the storage and the loss moduli, show a change from liquidlike to viscoelastic to elastic behavior during the sol−gel transition and vice versa during the gel−sol one. In situ EXAFS measurements performed at the Zr K-edge show that no change of the local order around Zr occurs during the sol−gel−sol transition, in agreement with the concept of physical gel formation. We have proposed for the structure of the precursor an inner core made of hydroxyl and oxo groups bridging together zirconium atoms surrounded in surface by complexing sulfate ligands. The sulfate groups act as a protective layer, playing a key role in the linking propagation among primary particles during sol−gel−sol transition.

1. Introduction

During the past decades, there has been considerable interest in the preparation of zirconia powders by the sol−gel process due to the good thermomechanical, catalytic, electrical, and optical properties of the zirconium-oxide based materials. Zirconium alkoxides, such as *n*-propoxide or *n*-butoxide, are generally used as precursors,[1−5] but due to the high reactivity of alkoxide precursors, the tailoring of the structural and microstructural characteristics of the sol−gel derived materials is very difficult. Some authors[3−5] have shown that the hydrolysis and condensation reactions could be controlled via chemical modification of the alkoxide precursors by using complexing ligands, which slow condensation reactions acting as surface protecting reagents. However, less attention has been directed for developing the sol−gel route starting from the inexpensive zirconyl chloride precursor ($ZrOCl_2 \cdot 8H_2O$). It is probably due to the difficulty in controlling the hydrolytic polymerization of these solutions. Clearfield[6] proposed a mechanism of hydrolytic polymerization of zirconyl chloride solutions and remarked that this difficulty may be bypassed by using chelating or complexing species as sulfate, oxalate, or glycol to change the polymerization pathway of the zirconium species.

Taking into account these results, we have begun a systematic study of the modification of zirconyl chloride aqueous solutions by sulfate anions, aiming to establish the experimental conditions for sol and gel formation. Surprisingly, we have observed that as the relation 3:1 $Zr:SO_4$ holds for the initial solution, the system presents a thermoreversible sol to gel transition. This behavior has not been reported for inorganic systems, in which the formation of covalent bonds allows a usually irreversible sol−gel transition. Besides, thermoreversible gels may be of striking interest because of their potential application in mechanical or optical switching, for instance.

(1) Sorec, Y.; Zevin, M.; Resfield, R.; Hurvits, J.; Ruschin, S. *Chem. Mater.* **1997**, *9*, 670−676.
(2) Suzuki, H.; Saito, H. *J. Mater. Sci.* **1990**, *25*, 2253−2258.
(3) Peter, D.; Ertel, T. S.; Bertagnolli, H. *J. Sol-Gel Sci. Technol.* **1995**, *5*, 5−14.
(4) Chatry, M.; Henry, M.; In, M.; Sanchez, C.; Livage, J. *J. Sol-Gel Sci. Technol.* **1994**, *1*, 233−240.
(5) Bartlett, J. R.; Woolfrey, J. L.; Percy, M.; Spiccia, L.; West, B. O. *J. Sol-Gel Sci. Technol.* **1994**, *2*, 215−220.
(6) Clearfield, A. *J. Mater. Res.* **1990**, *5* (1), 161−162.

S0897-4756(97)00387-6 CCC: $15.00
Published on Web 03/28/1998

Thermoreversible gels are two-phase systems, which acquire elastic properties under temperature changes. This behavior is often observed for organic systems such as proteins and polysaccharides in water and synthetic polymers in appropriate solvents.[7] The thermoreversibility may only be observed for physical gels, in which the connected network is due to physical interactions, i.e., hydrogen bonds and/or van der Waals forces. To our knowledge, just one article reports the formation of a thermoreversible gel in an inorganic system; it deals with aluminum and sodium polyphosphate, and gelation was attributed to the formation of a supramolecular network of polycations and polyanions.[8]

In this work we provide evidence for the thermoreversible sol−gel transition of zirconyl chloride aqueous solutions modified by sulfuric acid. Aiming to understand the mechanism responsible for this striking property, this transformation was followed by turbidity, rheology, and extended X-ray absorption fine structure (EXAFS) spectroscopy.

2. Experimental Section

2.1. Sample Preparation and Chemical Analyses. First, commercial $ZrOCl_2 \cdot 8H_2O$ powder (Aldrich) was dissolved in hydrochloric acid aqueous solution (0.01 mol L^{-1}). Next, colloidal suspensions were prepared by adding the acid $ZrOCl_2$ stock solution (0.21 mol L^{-1}, room temperature) to a hot (80 °C) aqueous solution of sulfuric acid (0.21 mol L^{-1}), drop by drop, under magnetic stirring. The volume of the $ZrOCl_2$ solution was adjusted to yield suspensions containing the 3:1 Zr^{4+}:H_2SO_4 molar ratio. Aliquots of 15 mL of the suspensions were put inside acetylcellulose membrane tubing (12−14 000 MW) and then submitted to static dialysis against 200 mL of bidistilled water during 24 h in order to obtain transparent and stable suspensions at pH 1.6. By adding base, these suspensions gelify at pH ∼2.7. We have also noted that an isochoric gelation may be obtained by increasing the temperature of the dialyzed sol above a critical temperature, T_c. Moreover, the liquefaction of the system was observed as the temperature decreases down to values smaller than T_c. The values of T_c are dependent on zirconium concentration, which was adjusted between 0.018 and 0.22 mol L^{-1} by aqueous dilution or vacuum evaporation at room temperature from the dialyzed suspension containing 0.156 mol L^{-1} of zirconium. This thermoreversible behavior is observed if the system is kept at temperatures 10 °C higher than T_c for a short period of time (less than 1 h). Irreversible gels are obtained by aging the gel with [Zr] = 0.156 mol L^{-1} at 80 °C for 4 h.

Information concerning the composition of the system was obtained from chemical analyses of freeze-dried samples: Zr content was determined by ICP/AES (inductive conduction plasma coupled to atomic emission spectroscopy), and S and Cl were determined by infrared detection during pyrolysis. We have also used the thermogravimetric analysis to determine the SO_3 and H_2O mass loss. The hydrosol and irreversible hydrogel were freeze-dried at −5 °C under 10^{-3} mm Hg vacuum in Janetzki MLW LGA05 equipment. The proposed minimal composition of the freeze-dried hydrosol and irreversible hydrogel so obtained is $Zr_6O_2(OH)_{12}(SO_4)_3Cl_2$. This result suggests that during dialysis the excess of chlorine ions was eliminated and that a small amount of zirconium was lost.

2.2. Samples Characterization. 2.2.1. Turbidimetric and Rheological Measurements. The thermal reversibility of the sol−gel transition was evidenced by recording the time evolution of the turbidity during the cycling of the isothermal temperature of the sample. The thermal cycling consisted of the following: the sol (at 20 °C) was placed into a thermostated cell at 56 °C, and the turbidity evolution was recorded during 120 min as a function of time; then, the sample was cooled at 20 °C, and the turbidity was recorded for 860 min; and so on. The effect of the zirconium concentration on the gel temperature was evaluated by measuring the turbidity of the samples during heating (rate = 1 °C min^{-1}) between 15 and 90 °C. Data collection was carried out using a Del Lab Nefelometer equipped with a special thermostated cell and tungsten polychromatic radiation.

The rheological measurements were done in an oscillatory shear mode with a Carri-Med CSL100 controlled stress rheometer, using the plate−plate geometry (radius 6 cm). The measurements were performed during the sol−gel transition at 56 °C and during the gel−sol transition at 20 °C. The temperature was kept constant (within 0.1 °C) by means of a Peltier device. The storage (G') and loss (G'') moduli of elasticity were recorded as a function of the transformation time at a fixed frequency (ω = 15 rad/s). In a parallel set of experiments these moduli were also measured as a function of the frequency ($0.1 < \omega < 63$ rad s^{-1}) after a given transformation time interval.

2.2.2. EXAFS Measurements. The EXAFS data at the Zr K-edge (17998 eV) were collected on the EXAFS I spectrometer at LURE (the French synchrotron radiation facility) using the DCI storage ring (1.85 GeV and positron currents of about 300 mA). The monochromator was a Si(331) channel-cut and the measurements were performed in the transmission mode using two ionization chambers filled with argon. The EXAFS spectra were recorded within a 1000 eV energy range with 2 eV steps and 1 s accumulation time per energy. Powdered samples were ground and placed between two layers of Kapton adhesive tape. The thermoreversible sol−gel transition for a solution with [Zr] = 0.156 mol L^{-1} was characterized by in situ experiment using a thermostated Teflon cell[9] possessing two Kapton windows and a variable optical path length. The thickness x of samples was chosen to obtain edge jumps of $\Delta\mu x \approx 1$. Data collection was carried out at constant temperature at 25, 40, and 60 °C.

2.3. EXAFS Data Analysis. All the EXAFS spectra were treated using the classical plane-wave single scattering approximation[10−14] according to the procedure described in ref 15. The main lines of this procedure are briefly summarized here. It has been performed on a microcomputer by using the chain of programs developed by Michalowicz.[16] Two references have been used herein: $Zr(SO_4)_2 \cdot 4H_2O$[17] and $ZrOCl_2 \cdot 8H_2O$[18] also abbreviated by the acronym ZOC. $Zr(SO_4)_2 \cdot 4H_2O$ has in its first coordination shell eight oxygen atoms located from the absorbing zirconium atom at 2.18 Å.[17] The ZOC structure is based on the $[Zr_4(OH)_8(H_2O)_{16}]^{8+}$ tetranuclear complex in which each zirconium atom is surrounded by four bridging OH ligands at the mean distance 2.142 ± 0.019 Å and by four terminal H_2O molecules at the mean distance 2.272 ± 0.032 Å.[18] In this tetrameric structure, the second nearest neighbors are two zirconium atoms linked to the absorbing atom by double hydroxo bridges and located at 3.559 Å.

After atomic absorption removal and normalization, the $k^3\chi(k)$ weighted EXAFS signal was Fourier transformed to R distance space, using the 3.3−14.5 $Å^{-1}$ Kaiser apodization

(7) Djabourov, M. *Rev. Gén. Therm. Fr.* **1987**, *306&307*, 369−373.
(8) Lima, E. C. O.; Galembeck, F. *J. Colloid Interface Sci.* **1994**, *166*, 309−315.
(9) Villain, F.; Briois, V.; Castro, I.; Helary, C.; Verdaguer, M. *Anal. Chem.* **1993**, *65*, 2545−2548.
(10) Sayers, D. E.; Stern, E. A.; Lytle, F. W. *Phys. Rev. Lett.* **1971**, *27*, 1204−1207.
(11) Kincaid, B. M.; Eisenberger, P. *Phys. Rev. Lett.* **1975**, *34*, 1361−1364.
(12) Ashley, C. A.; Doniach, S. *Phys. Rev. B* **1975**, *11*, 1279−1288.
(13) Lee, P. A.; Pendry, J. B. *Phys. Rev. B* **1975**, *11*, 2795−2811.
(14) Teo, B. K. *EXAFS: Basic Principles and Data Analysis*; Springer-Verlag: Berlin, 1986.
(15) Briois, V.; Santilli, C. V.; Pulcinelli, S. H.; Brito, G. E. S. *J. Non-Cryst. Solids* **1995**, *191*, 17−28.
(16) Michalowicz, A. *EXAFS pour le Mac, Logiciels pour la Chimie*, Société Française de Chimie: Paris, 1991; p 102.
(17) Singer, J.; Cromer, D. T. *Acta Crystallogr.* **1959**, *12*, 719−723.
(18) Mak, T. C. W. *Can. J. Chem.* **1968**, *46*, 3493−3497 and ref 1 therein.

window with $\tau = 2.5$. The contributions of the various shells of neighbors were extracted by a back Fourier transform in R space and then fitted using experimental or theoretical phase and amplitude functions, depending on the considered backscatterer. So the phase shift for the Zr−O pair and the oxygen backscattering amplitude were extracted from the $Zr(SO_4)_2 \cdot 4H_2O$ reference[17] backtransforming the first peak of its Fourier transform (FT) and setting $N = 8$, $R = 2.18$ Å and $\sigma = 0.065$ Å. This Debye−Waller factor was determined by fitting first the filtered for $Zr(SO_4)_2 \cdot 4H_2O$ signal using the theoretical function as reported in the McKale's tables.[19] This approach allows one to obtain the experimental amplitude function not convoluted with the Debye−Waller term but still convoluted with the mean free path. For Zr backscattering atoms, we have preferred to use theoretical amplitude and phase functions[19] rather than those extracted from the $ZrOCl_2 \cdot 8H_2O$ reference. Although both sets of functions gave similar results in the fitting of Zr contributions, the best fits were obtained with the theoretical functions. The structural parameters for sol and gel samples were obtained by two different methods, as described below.

2.3.1. Least-Square Fitting (Method I). The coordination numbers N_j, the distances R_{ij}, and the Debye−Waller factors σ_j, were obtained using a least-squares procedure by keeping fixed the parameter Γ, related to the mean free path of the photoelectron, and the threshold energy E_0 at the values determined previously on the $ZrOCl_2 \cdot 8H_2O$ reference for each contribution: $\Gamma = 0$ and $E_0 + \Delta E_0 = 18022 \pm 0.5$ eV for the oxygen contribution, $\Gamma = 1.41$ and $E_0 + \Delta E_0 = 18\,007 \pm 0.5$ eV for the zirconium contribution. The procedure of adjustment was performed in two steps: first, the Zr−O contribution was simulated, and then the Zr−O and Zr−Zr contributions were fitted simultaneously. To avoid correlation between the oxygen coordination number and the number of zirconium neighbors, the structural parameters related to the oxygen contribution were carefully kept to the values previously obtained, only the structural parameters for the Zr−Zr contribution being simulated. The reliability of the fit is determined by the agreement factor ρ:

$$\rho = \frac{\sum_i (\chi^i_{\mathrm{exp}}(k_i) - \chi^i_{\mathrm{calc}}(k_i))^2}{\sum_i (\chi^i_{\mathrm{exp}}(k_i))^2} \qquad (1)$$

2.3.2. Amplitude Ratio Comparison (Method II). The coordination number can also be determined by using the amplitude ratio method,[20] which is based on the comparison of the experimental amplitudes obtained from the inverse Fourier transforms of the unknown sample and a reference of known structure, $A_a(k)$ and $A_b(k)$, respectively. The ratio between the envelopes $A(k)$ of both EXAFS signals is deduced from the EXAFS formula[20, 21]

$$A_a(k)/A_b(k) = [N_a/N_b][R_b/R_a]^2[F_a(k)/F_b(k)] \times [\exp(-2\sigma_a 2k^2)/\exp(-2\sigma_b 2k^2)] \qquad (2)$$

where all multielectron and inelastic effects have been included in $F(k)$. For an appropriate reference, for which $F_b(k)$ is comparable to $F_a(k)$, the plot of $\ln(A_a(k)/A_b(k))$ vs k^2 will be a straight line with a slope of $2\Delta\sigma^2 = 2(\sigma_b^2 - \sigma_a^2)$ and an intercept of $\ln([N_a/N_b][R_b/R_a]^2)$. For samples having the same R distances, the method gives directly the disorder and the coordination number for the unknown samples.

3. Results

Figure 1 shows the evolution of the turbidity of the sample containing [Zr] = 0.156 mol L^{-1} as a function of the time during the thermal cycles shown at the top of this figure. Simultaneous with the increase of the turbidity, one observes a macroscopic increase of the viscosity leading to the gelation of the system during the isothermal treatment at 56 °C. Both the turbidity and the viscosity decrease resulting in a liquefaction of the gel during the subsequent isothermal treatment at 20 °C. This behavior is similar to the thermoreversible sol−gel transition observed for biological and polymeric systems.[7] As shown in Figure 1 for each cycle, the increase of the turbidity is faster than its decrease, resulting in an hysteresis loop. Moreover, the maximum and the minimum of the turbidity increase continuously with the thermal cycles. It indicates that there are some changes on the suspension characteristics and that the sol−gel transition is partially thermoreversible.

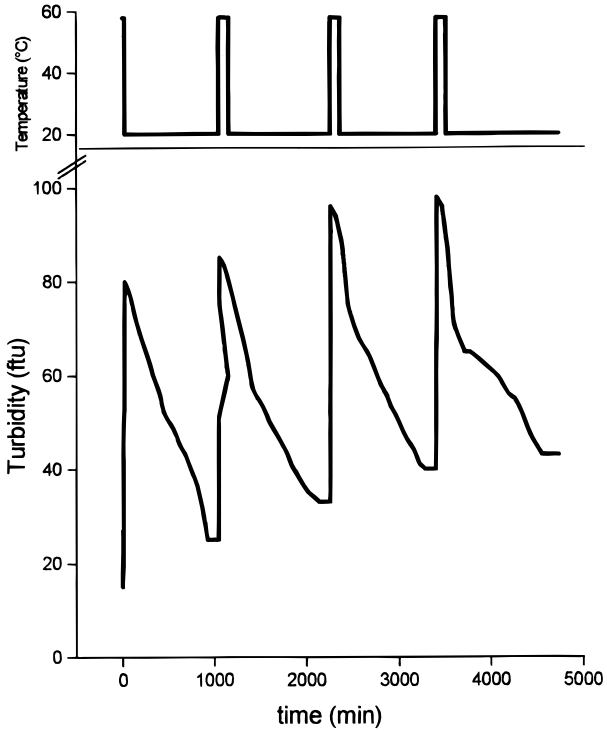

Figure 1. Evolution of the turbidity as a function of the time during the thermal cycles (shown at the top) for the sample containing [Zr] = 0.156 mol L^{-1}.

The effect of the zirconium concentration on the evolution of the turbidity during heating at 1 °C min^{-1} is shown in Figure 2. All the curves present a sigmoidal shape, analogous to that observed for thermostimulated phase transitions. The critical transformation temperature (estimated by the intersection of dashed straight lines) increases from 50 to 80 °C as the concentration of zirconium decreases from 0.22 to 0.018 mol L^{-1}. Furthermore, gelation is achieved only for [Zr] ⩾ 0.156 mol L^{-1} while for lower concentrations the viscosity increases but gelation does not occur.

The time evolution of the storage (G') and loss (G'') moduli of elasticity (for sample containing [Zr] = 0.156 mol L^{-1}) as a function of the time measured at a fixed angular frequency ($\omega = 15$ rad s^{-1}) during the isother-

(19) McKale, A. G.; Veal, B. W.; Paulikas, A. P.; Chan, S. K.; Knapp, G. S. J. *J. Am. Chem. Soc.* **1988**, *110*, 3763−3768.

(20) Sayers, D. E.; Stern, E. A.; Lytle, F. W. *Phys. Rev. Lett.* **1975**, *35*, 584−587.

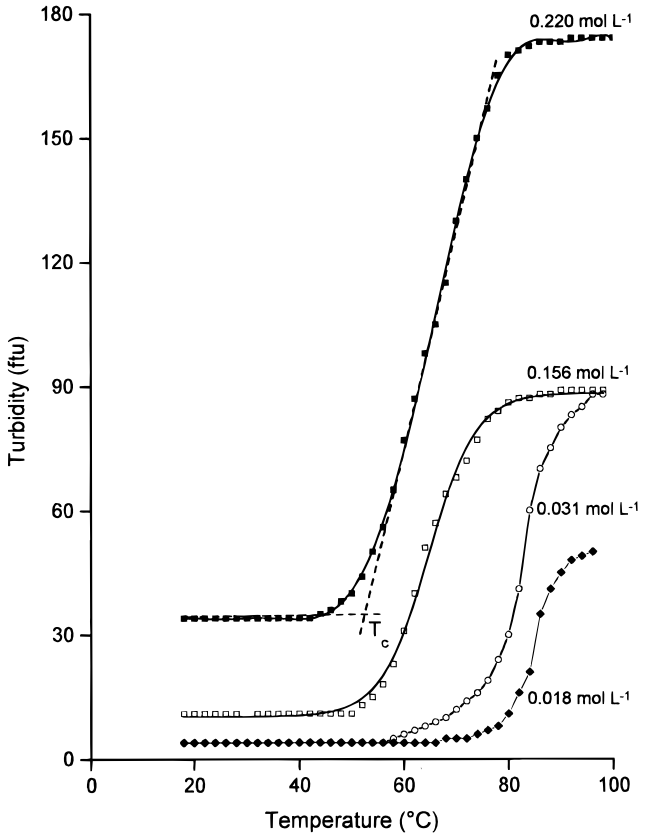

Figure 2. Effect of the zirconium concentration on the evolution of the turbidity during heating at 1 °C min^{-1}. The intersection of dashed straight lines illustrates the critical transformation temperature, T_c, determination.

mal sol−gel transition at 56 °C and during the gel−sol transition at 20 °C is presented in parts a and b of Figure 3, respectively. Concerning the sol−gel transition, G' increases faster than G'', the crossover occurring after 120 min, in good agreement with the time observed for the visual gelation of a standard sample maintained at the same temperature. In the case of the gel−sol transition, the crossover is only observed after 460 min.

The storage (G') and loss (G'') moduli of elasticity as a function of the angular frequency (ω) measured at different stages of the sol−gel transition at 56 °C and the gel−sol transition at 20 °C are presented in the log−log plot in parts a and b of Figure 4, respectively. Before gelation the power-law dependence between the moduli and the angular frequency are typical of liquidlike systems, and after that G' and G'' become frequency independent, characteristic of solidlike systems. Inverse behavior is observed during the gel−sol transition.

The EXAFS signals and their FTs recorded during the sol−gel and gel−sol transitions are compared to the solid reference $ZrOCl_2 \cdot 8H_2O$ (ZOC) in parts a and b of Figure 5, respectively. The samples were named to describe their physical state and the temperature at which the EXAFS spectra were recorded as follows: (i) at room temperature (25 °C) and in the sol state, SOL-RT1; (ii) at 40 °C and still in the sol state, SOL-40; (iii) at 60 °C and in the gel state: GEL-60. Each sample was measured 5 times and the presented data are the sum of these five scans. Finally, about 18 h after the sol−gel transition, when the system has come back to room temperature and then in the sol state, we have

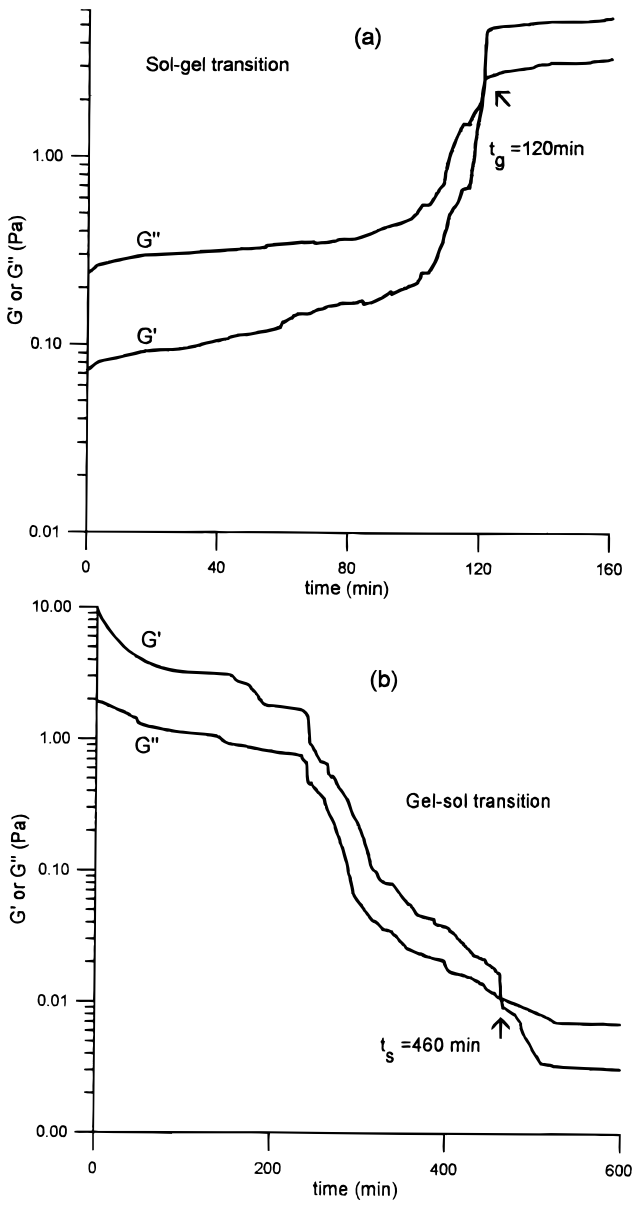

Figure 3. Time evolution of the storage (G') and loss (G'') moduli of elasticity as a function of the time at a fixed angular frequency ($\omega = 15$ rad s^{-1}) measured (a) during the isothermal sol−gel transition at 56 °C and (b) during the gel−sol transition at 20 °C.

recorded three spectra: they deal with the sample called SOL-RT2. Very similar shapes of EXAFS signals are observed for the ZOC reference and for the samples, except in the k range between 6 and 8 $Å^{-1}$ in which the spectra of sol and gel samples show a plateau in the minimum of the concerned EXAFS oscillation. The FTs present two main peaks located at the same R distance in the reference and in the samples. According to the ZOC crystal structure, peak A is attributed to the first oxygen coordination sphere around Zr and peak B to the zirconium atoms located at longer distances. A casual examination of the intensities and shapes of the spectra seems to indicate that no important structural modifications around the absorbing zirconium occur during the reversible sol−gel transition. For the first three samples, one observes only a small decrease of intensities of both peaks of the FTs when the temperature is raised. This behavior is due to an increase of

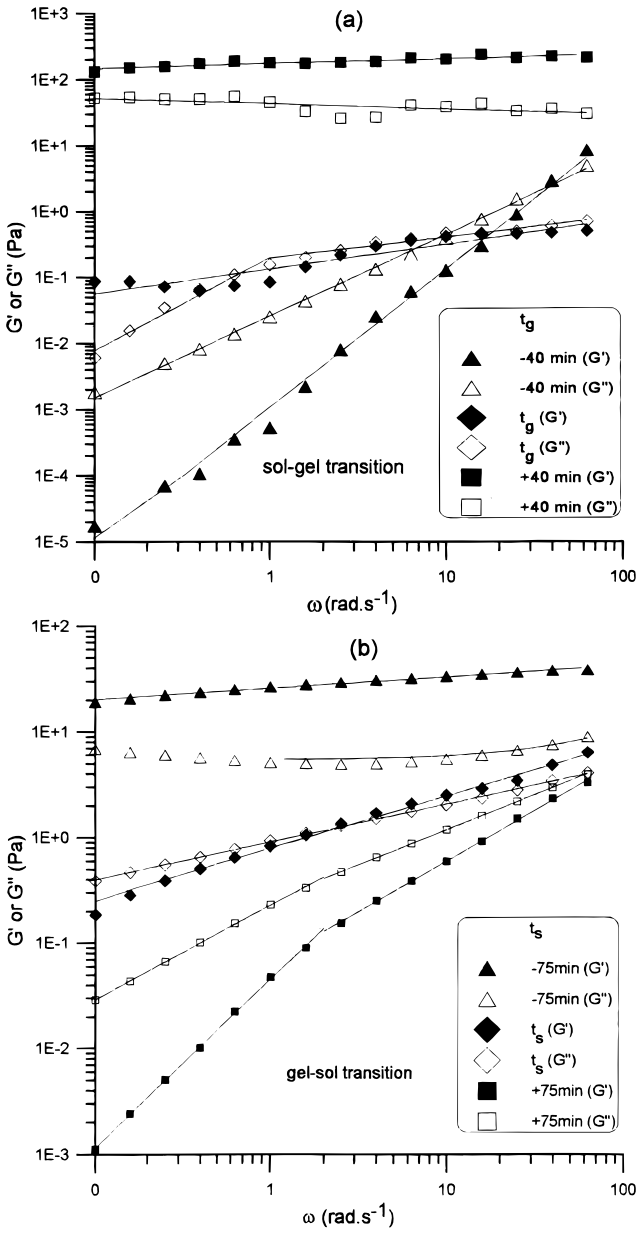

Figure 4. Evolution of the storage (G') and loss (G'') moduli vs angular frequency (ω) at successive times (a) during sol−gel at 56 °C and (b) during gel−sol transition at 20 °C.

the thermal part of the Debye−Waller factor as verified by the least-squares fit of the data.

The comparison between experimental and theoretical curves is presented in Figure 6 for the ZOC reference and one of the samples, the SOL-RT1. As the fitting procedure was initially based on separate simulations of peak A and peak B, we have reported on the same figure the curves fitting each contribution. For all the samples, it was impossible to fit the data relative to the first coordination sphere with only one Zr−O distance, and two subshells have to be used. As reported in Table 1, two oxygen distributions fit satisfactorily the data: 3.0 atoms at 2.13 Å and 4.0 atoms at 2.24 Å (Model 1) or 4.0 atoms at 2.14 Å and 3.0 atoms at 2.27 Å (Model 2). The differences between both models lie, on one hand, on the values of the Debye−Waller factors which are reasonable in both cases and, on the other hand, on the average distances which are faintly shifted. The statistical errors on the determination of the structural

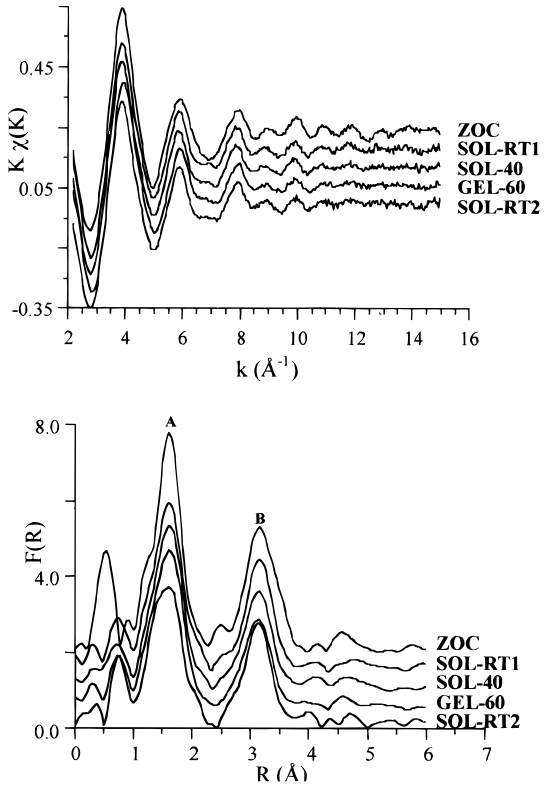

Figure 5. (a) Experimental $k\chi(k)$ vs k EXAFS signals and (b) amplitude of the Fourier transforms of $k^3\chi(k)$ for the sol and gel samples labeled SOL-RT1, SOL-40, GEL-60, SOL-RT2 (see the text) and for the model compound $ZrOCl_2 \cdot 8H_2O$ labeled ZOC. For clarity, each curve in both figures was shifted upward by a constant with regard to the preceding one.

parameters were estimated to be ±0.02 Å in distance and ±10% in coordination numbers and Debye−Waller factors. But the existence of these two possible oxygen distributions of almost equal reliability for these samples indicates that the errors on the numbers of neighbors and Debye−Waller factors are larger and close to 25% for these compounds. A plausible explanation for the existence of these two models will be given in the discussion. As expected, the disorder inside both shells, quantified by the Debye Waller factors, increases faintly with the increase of the temperature. Furthermore, the disorder, at least in the first oxygen coordination shell, exists always after the transition when the system has come back at room temperature. This is a manifestation of the hysteresis phenomenon evidenced by the turbidimetric measurements.

Concerning the simulation of the zirconium contribution, the best simulation of peak B has been achieved with one shell of 6.5 ± 0.6 zirconium atoms located at 3.57 ± 0.02 Å. This number of Zr neighbors is very high compared to the two Zr neighbors in ZOC or to the usual numbers of Zr neighbors for other basic zirconium salts.[22−25] To remove any ambiguity, the number of Zr neighbors was also determined by the amplitude ratio (method II), the chosen references being $ZrOCl_2 \cdot 8H_2O$

(21) Gurman, S. J. *J. Synchrotron Rad.* **1995**, *2*, 56.
(22) McWhan, D. B.; Lundgren, G. *Inorg. Chem.* **1966**, *5*, 284−289.
(23) Hansson, M. *Acta Chem. Scand.* **1973**, *27*, 2614−2622.
(24) El Brahimi, M.; Durand, J.; Cot, L. *Eur. J. Solid State Inorg. Chem.* **1988**, *25*, 185−189.
(25) Gascoigne, D.; Tarling, S. E.; Barnes, P.; Pygall, C. F.; Bénard, P.; Louer, D. *J. Appl. Crystallogr.* **1994**, *27*, 399−405.

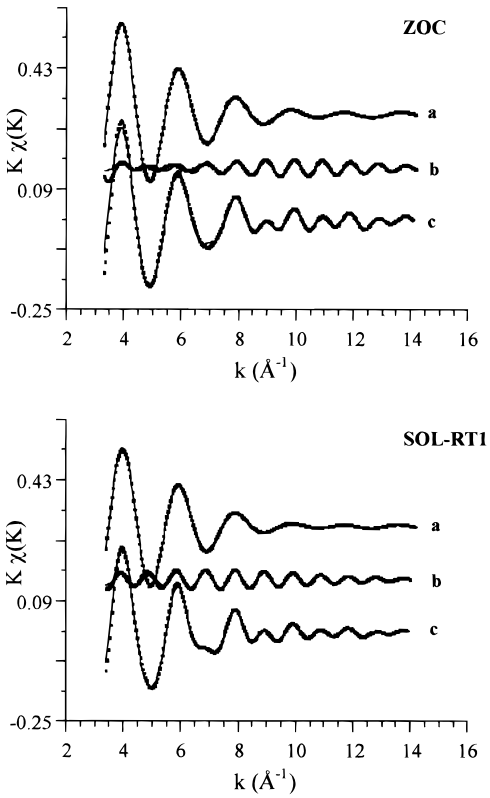

Figure 6. Fit (full line) of the Fourier filtered signals (dotted line) for SOL-RT1, according to model 1, and the ZOC reference: (a) first oxygen contribution only, (b) second zirconium contribution only, and (c) first and second contribution together. For clarity, each contribution was shifted upward by a constant with regard to the preceding one.

with $N_b = 2$ zirconium atoms at $R_b = 3.56$ Å, for the powdered freeze-dried hydrosol and hydrogel samples, which have the same R distances. A satisfactory linear behavior for all the samples characterized by EXAFS was achieved for k^2 ranging from 60 to 150 Å^{-2}. We can observe in Table 1 that both sets of parameters obtained by both methods I and II are in good agreement.

Finally, it is noteworthy that the peculiar shape of the minimum of the EXAFS oscillation between 6 and 8 Å^{-1} observed for the sol and gel samples is related to the number of zirconium neighbors. As seen in Figure 6, this k range corresponds to a maximum of the zirconium contribution, leading to the appearance of a step in the middle of this oscillation and a plateau for the signal. It deals with a fingerprint of the Zr−Zr contribution; and the more Zr atoms in the second shell there are, the sharper this step in the middle of the oscillation becomes.

4. Discussion

Discussion is given in three parts, the first one, involving the phenomenological description of the thermoreversible sol−gel−sol transition, is based on the turbidimetric and rheological behavior; the second, based on EXAFS, focuses on the structural characteristics of this system; the last gives a structural explanation for the thermoreversible gelation.

4.1. Turbidimetric and Rheological Behavior. The turbidimetric measurements (Figures 1 and 2) evidence the partial thermoreversibility of the sol−gel transition for zirconyl chloride aqueous solutions modified by sulfuric acid. The turbidity is highly dependent on the scattering cross-section of particles in suspension,[26] and the observed increase in turbidity during heating must be related to the growth of the forming macromolecules or aggregates. Furthermore, the decrease in turbidity after cooling could be associated with solubilization of macromolecules or desaggregation. This behavior is in agreement with a previous small angle X-ray scattering (SAXS) study[27] performed with samples containing [Zr] = 0.156 mol L^{-1}, which has shown that the size of the primary particles in the sol is 0.6 nm. Aggregation results in a fractal structure of about 3 nm correlation length. Before gelation, swelling of the fractal structure occurs and the interface area between solvent and aggregates does not change during the sol−gel transition. Moreover, the partial behavior of the thermoreversibility evidenced by the increase of the minimum and maximum values of the turbidity as the number of thermal cycles increases (Figure 1) shows that, by cycling, the size of elementary aggregates increases progressively due to the formation of some strong interactions, which are not totally destroyed during liquefaction.

The reversibility of the sol−gel transition was also put in evidence by the kinetic evolution of the storage and loss moduli of elasticity. At the beginning of the isothermal treatment at 56 °C, the loss modulus (G'') is higher than the storage modulus (G'), characterizing a liquidlike behavior[28] (Figure 3). At this same time interval, the frequency sweep has shown a power-law dependence between the moduli and the frequency ($G'(\omega) \propto \omega^{\Delta'}$; $G''(\omega) \propto \omega^{\Delta''}$), the exponent values being $\Delta' = 2$ and $\Delta'' = 1$, confirming the liquidlike behavior[29] (Figure 4). In the early stage of the sol−gel transition, both the moduli increase and no delay is observed between them. It corresponds to a simultaneous increase of the real part of the dynamic viscosity due to the increasing molecular weight of forming macromolecules or of aggregates size and to the network formation.[28] This simultaneous increase of G' and G'' is generally observed as the system has already some particles or aggregates in solution, and the tridimensional network results from the first interlinkages among them.[30] This behavior is in agreement with the cluster−cluster aggregation mechanism evidenced by SAXS.[27] G' increases faster than G'', rapidly overlapping the G'' curve, and the observed crossover may correspond to the gel point. In fact, the frequency sweep (Figure 4) shows a plateau of $G''(\omega)$ at high frequency ($2 < \omega < 100$ rad/s), characterizing a viscoelastic regime due to gel formation. These behaviors are generally used as a criteria to fix the gel time.[29]

After the gel time both G'' and G' reach a plateau, G' being always higher than G'' (Figure 3) and becoming

(26) Dos Ramos, J. G.; Silbi, C. A. *J. Colloid Interface Sci.* **1990**, *135*, 165−173.
(27) Chiavacci, L. A.; Pulcinelli, S. H.; Santilli, C. V.; Craievich, A. F. *J. Appl. Cryst.* **1997**, *30*, 750−754.
(28) Ward, I. M. *Mechanical Properties of Solid Polymers*, 2nd ed.; Wiley-Interscience Publ.: U.K., 1985; Chapter 5.
(29) Djaburov, M.; Lebond, J.; Papon, J. *J. Phys.* **1988**, *49*, 333−343.
(30) Lacan, P.; Guizard, C.; Cot, L. *J. Sol-Gel Sci. Technol.* **1995**, *4*, 151−162.

Table 1. Structural Parameters Determined during the Sol−Gel and Gel−Sol Transition[a]

	method I, model 1				method I, model 2				method II	
sample	N_i	σ_i (Å)	R_i (Å)	ρ (%)	N_i	σ_i (Å)	R_i (Å)	ρ (%)	N_{Zr}	σ_{Zr} (Å)
ZOC	4.1 O	0.058	2.13	(0.11)	4.1 O	0.058	2.13	(0.11)		
	4.1 O	0.094	2.26		4.1 O	0.094	2.26			
	2.0 Zr	0.057	3.57	1.44	2.0 Zr	0.057	3.57	1.44		
SOL-RT1	3.0 O	0.063	2.13	(0.12)	4.0 O	0.063	2.13	(0.10)		
	4.1 O	0.095	2.24		2.9 O	0.075	2.27			
	6.2 Zr	0.098	3.57	0.70	6.1 Zr	0.095	3.57	0.80	5.7	0.100
SOL-40	3.0 O	0.064	2.13	(0.06)	4.0 O	0.067	2.13	(0.06)		
	4.1 O	0.095	2.24		2.9 O	0.078	2.27			
	6.4 Zr	0.101	3.58	0.76	6.3 Zr	0.101	3.57	0.79	6.5	0.104
GEL-60	3.0 O	0.064	2.13	(0.11)	4.1 O	0.070	2.14	(0.12)		
	4.0 O	0.096	2.24		2.9 O	0.089	2.27			
	6.6 Zr	0.106	3.58	0.67	6.8 Zr	0.106	3.58	0.64	6.5	0.106
SOL-RT2	3.1 O	0.070	2.14	(0.31)	4.1 O	0.074	2.14	(0.29)		
	4.1 O	0.111	2.24		3.0 O	0.097	2.28			
	6.1 Zr	0.100	3.57	0.85	6.0 Zr	0.100	3.57	0.90	7.0	0.101
freeze-dried hydrosol	2.9 O	0.065	2.12	(0.19)	4.0 O	0.073	2.14	(0.18)		
	3.8 O	0.091	2.24		2.8 O	0.092	2.27			
	6.4 Zr	0.109	3.57	1.19	5.7 Zr	0.107	3.55	0.81	6.3	0.110

[a] Method I corresponds to the least-squares fitting procedure. Two distributions, model 1 and model 2, for the oxygen contribution are possible with almost equal reliability. The agreement factor in parentheses is related to the fit of the first oxygen coordination shell, whereas the other value is the agreement factor for the three-shell fitting procedure. Method II corresponds to the amplitude ratio method applied between 60 and 150 $Å^{-2}$.

frequency-independent (Figure 4), confirming the predominant elastic character of the gel and proving that a real tridimensional network has been formed.[7] In general, G' increases continuously during aging due to the increase of cross-link density for chemical gels or to the increase of single points or junction zones bonding for physical gels.[7,29] Besides, the plateau of G' evidences that the network connectivity does not increase more after gelation.

During the gel−sol transition (20 °C), even in the gel state we could observe several decreasing steeps in G' curve, which are not clearly evident in G'' curve (Figure 3). It indicates that the decrease of the network connectivity is not continuous, what could be attributed to a strong difference in intensity of the interactions at the points or zones of junction. Following, G' and G'' decrease simultaneous and abruptly, characterizing both the decrease of the network connectivity and of the size of the formed clusters.[29] The curves reach a crossover point characteristic of liquefaction, and after that G' becomes smaller than G'' as in liquid systems. After the liquefaction time, the frequency sweep (Figure 4) shows that both G' and G'' become frequency-dependent, characterizing the transition from elastic to liquidlike behavior.[28]

The above discussion evidences that this system is thermoreversible both from the turbidimetric and rheological points of view. Furthermore, it gives evidences that the network is formed by the connectivity of primary clusters, in which the intensity of physical interlinkages varies from one point of junction to the other.

4.2. Structural Characteristics. The in situ EXAFS results show that no changes of the local order around Zr occur during the sol−gel−sol transition, except for an increase of the thermal part of the Debye−Waller. It agrees well with the concept of the formation of physical gels, where the network is not formed by covalent linkages. The EXAFS analysis reveals clearly for the primary particles the formation of a structure different from the one reported for ZOC, i.e. the cyclic tetramer $[Zr_4(OH)_8(H_2O)_{16}]^{8+}$, which is generally[6] formed in analogous aqueous acid solutions in absence of complexing anions. Although the EXAFS signals of the ZOC reference and the samples are similar, the two different methods used for the determination of the number of Zr neighbors in zirconium shells at 3.57 Å give undoubtedly 6.5 ± 0.6. This number is very different from the two Zr atoms located at the same distance for the ZOC reference. The high number of Zr neighbors found in our samples also excludes the formation of some reported basic zirconium sulfates:[22−24] $Zr_2(OH)_2(SO_4)_3(H_2O)_4$, $Zr(OH)_2SO_4 \cdot H_2O$, and $Zr(OH)_2SO_4$, in which the absorbing Zr atoms is also surrounded by two zirconium atoms at the same average distance of 3.56 Å.

The high number of zirconium neighbors revealed by EXAFS suggests (i) the formation of a tridimensional structure, in which the inner shell is formed by hepta-coordinated oxygen polyhedra and (ii) that the connectivity between the polyhedra is supported by oxygen bridging linking Zr atoms, leading to the formation of a ZrO_2-like core. This kind of structure is commonly found after hydrolytic polymerization of zirconium alkoxide chemically modified by complexing ligands such as acetylacetonate.[4] In the specific case of $Zr:SO_4$ ratio > 1, the sulfate complexing ligands play a role similar to the one reported for acetylacetonate ligands, i.e., they act as a surface protecting reagent controlling the condensation of primary particles. For example, such surface complexation of sulfate ligands is encountered in the $Zr_{18}O_4(OH)_{38.8}(OSO_3)_{12.6}$ compound for which the single-crystal structure has been recently refined.[31] The inner core of the molecule is made only of hydroxyl and oxo groups bridging together zirconium atoms whereas the sulfate ligands are located at the surface of this $Zr(OH)_xO_y$ core. A careful analysis of this structure evidences good agreement with our EXAFS results as shown below.

(31) Squattrito, P. J.; Rudolf, P. R.; Clearfield, A. *Inorg. Chem.* **1987**, *26*, 6, 4240−4244.

The Zr−O distances involved in the $Zr_{18}O_4(OH)_{38.8}(OSO_3)_{12.6}$ structure present a large distribution from 2.04 to 2.42 Å, revealing two asymmetric contributions of the oxygen ligands: the first one is centered at 2.12 Å with a mean coordination number of 3.6 oxygen atoms per zirconium atom, the second one is centered at 2.25 Å with a mean coordination number of 4.2 oxygen atoms per zirconium. The first group consists of 88% of doubly and triply bridging oxygen atoms whereas the second one is made for the half to sulfate or water molecules. The distribution of distances in the second group (from 2.20 to 2.42 Å) is almost twice larger than in the first group (from 2.04 to 2.18 Å). Furthermore, concerning the nearest zirconium atoms, we found for this complex an average distance of 3.576 Å, with distances ranging from 3.416 to 3.684 Å and a mean number of 4 for the Zr neighboring.

With the Zr−O distance distribution in mind, we better understand both models that are able to fit the EXAFS data. Depending on the choice of the limits of the asymmetric oxygen distribution, it is possible to shift the mean coordination number, the Debye−Waller factor, and the average distance for each shell. Both models used to fit the first oxygen contribution of the EXAFS spectra are in good agreement with the structure of $Zr_{18}O_4(OH)_{38.8}(OSO_3)_{12.6}$, considering the accuracy of the technique and the large distribution of distances for this compound. Dealing with the fit of the zirconium contribution, the Zr−Zr distance found by EXAFS agrees well with the average distance in the $Zr_{18}O_4(OH)_{38.8}(OSO_3)_{12.6}$ compound. The larger mean number of zirconium neighbors (6.5 ± 0.6) obtained by EXAFS would indicate for the primary particles a larger polynuclear cluster involving more triply and quadruply bridging oxide ions. Finally, it is noteworthy that the synthesis route used to prepare this single crystal[31] (prepared with the composition 1.43:1 $Zr:SO_4$) is very similar to the procedure we have adopted. Furthermore, the chemical composition of the freeze hydrosol agrees fairly well with the EXAFS interpretation based on the formation of primary particles of highly polynuclear species such as the known $Zr_{18}O_4(OH)_{38.8}(OSO_3)_{12.6}$ compound.[31]

4.3. On the Thermoreversible Gelation. Considering the above structural molecular model, we propose the following explanation for the thermoreversible gelation. The sulfate groups, which are at the surface of the molecular primary unit, may act as a protective layer due to the electronic density of the terminal sulfate oxygen atoms compensated by the positive charge of the hydronium ions (pH = 1.6). It will induce the structure building of water molecules hindering the interactions among the primary particles. Upon heating, the interfacial water layers should become less structured due to the decrease of the dielectric constant of water and to the exothermic characteristic of the hydration reactions. In other words, heating decreases the extent of solvation around the primary units and increases the electrostatic potentials, allowing more intense interactions between particles. As a consequence, the propagation of linking between primary particles could be supported by hydrogen bonds between terminal sulfate oxygen atoms and water molecules as proposed by Squattrito et al.[31] This leads to gelation of the system. Reciprocally, by decreasing the temperature, these weak linkages are perturbed by the increase of solvation leading to liquefaction.

The partial thermoreversibility observed by turbidimetric and rheological measurements indicates that some strong linkages between particles occur, probably involving sulfate bridging ligands. The amount of these covalent interactions increases both with time and temperature. In fact, as reported by Clearfield,[32] these sulfate groups play a determinant role in the development of the oxide network. Experimental evidences for this idea have been gained with the IR study of the irreversible hydrogel and with the kinetic EXAFS study of the formation of the irreversible gel,[33] which shows an increase in the bridging character of the sulfate ligands in the hydrogel sample. Moreover, the Zr−O distances in the irreversible gels are clearly shifted to shorter distances with regard to the distances in the reversible system, becoming comparable to the average Zr−O distances for the monoclinic ZrO_2 phase.

From the applied point of view, the strong dependence of the turbidity with the temperature confers to this system interesting properties with potential use in thermal optical devices as smart windows. In particular, the possibility of decreasing the critical temperature near the room temperature by acting on the zirconium concentration can be used to control the energy transfer across windows of residential and commercial buildings. Nevertheless, the fact that this phenomenon is partially thermoreversible hinders an immediate development of these devices.

5. Conclusions

We have put in evidence the first inorganic sol−gel thermoreversible transition for a nonpolyelectrolyte system. It consists of zirconyl chloride aqueous solutions modified by sulfuric acid in the ratio 3:1 $Zr:SO_4$. We have shown that the critical gelation temperature can be controlled by the zirconium concentration.

The ability of the sulfate anions to strongly complex the zirconium aqueous precursors play a key role in the stability of the sol and on the thermoreversible behavior of the gelation.

Indeed, the sol is composed by primary particles built up from ZrO_2-like core surrounded in surface by complexing sulfate ligands. Due to the electrostatic interactions involving the sulfate layer and the acid medium, the sol is stable at room temperature.

The dependence of the solvation with the temperature allows the formation of the gel network through the formation of weak linkages between primary particles.

Acknowledgment. This work has been financially supported by the FAPESP (Brazil) and by a CAPES/COFECUB cooperation program between Brazil and France.

CM970387D

(32) Clearfield, A.; Serrette, G. F.; Khazi-Syed, A. H. *Catal. Today* **1994**, *20*, 295−312.
(33) Chiavacci, L. A.; Pulcinelli, S. H.; Santilli, C. V.; Briois, V. Work in progress.